Journal of Alloys and Compounds 480 (2009) 947–953

Contents lists available at ScienceDirect

Journal of Alloys and Compounds

journal homepage: www.elsevier.com/locate/jallcom

On the $Fe_3O_4/Mn_{1-x}Zn_xFe_2O_4$ core/shell magnetic nanoparticles

R.Y. Hong[a,b,*], J.H. Li[a], X. Cao[a], S.Z. Zhang[a], G.Q. Di[c], H.Z. Li[b], D.G. Wei[d]

[a] College of Chemistry, Chemical Engineering and Materials Science & Key Laboratory of Organic Synthesis of Jiangsu Province, Soochow University, SIP, Suzhou 215123, China
[b] State Key Laboratory of Multi-phase Complex Systems, Institute of Process Engineering, Chinese Academy of Sciences, Beijing 100080, China
[c] Department of Physics, Soochow University, Suzhou, 215007, China
[d] Center for Nanoscale System, School of Engineering & Applied Science, Harvard University, 11 Oxford Street, Cambridge, MA 02139, USA

ARTICLE INFO

Article history:
Received 8 December 2008
Received in revised form 19 February 2009
Accepted 20 February 2009
Available online 5 March 2009

Keywords:
Composite materials
Oxide materials
Chemical synthesis
Magnetic measurements

ABSTRACT

Fe_3O_4 magnetic nanoparticles (NPs) were synthesized by the co-precipitation of Fe^{3+} and Fe^{2+} with ammonium hydroxide under hydrazine hydrate, and were characterized by X-ray powder diffraction (XRD), transmission electron microscopy (TEM) and vibrating sample magnetometer (VSM). In order to improve the particle dispersion, the bare Fe_3O_4 magnetic NPs were surface modified by sodium citrate under Ar protection. Mn–Zn ferrite NPs were prepared by co-precipitation. A group of orthogonal tests ($L4^5$) were arranged to investigate the effects of reaction temperature, and OH^- and Fe^{3+} concentrations on the magnetic property of Mn–Zn ferrite. It was found that the saturation magnetization increases evidently with the increasing reaction temperature. The effects of OH^- and Fe^{3+} concentrations on the magnetic property are minor. Mn–Zn ferrite NPs with high saturation magnetization (53 emu/g) were obtained.The XRD and element analysis for the Mn–Zn ferrite NPs indicates the particles are pure $Mn_{0.8}Zn_{0.2}Fe_2O_4$. Finally, $Fe_3O_4/Mn_{0.8}Zn_{0.2}Fe_2O_4$ core/shell nanocomposites were prepared by co-precipitation under the same condition. The core/shell nanocomposites obtained in the optimal condition demonstrate the highest saturation magnetization of 68 emu/g.

1. Introduction

Magnetite (Fe_3O_4), an important member of spinel type ferrite, is widely used in mineral separation [1], heat transfer applications [2], electrophotography [3], efficient hyperthermia for cancer removal [4], therapy, pharmacy, biosensors [5,6], MRI contrast agents [7,8], dynamic sealing [9], orientation control and directional transportation [10], and so on. Methods about synthesis of Fe_3O_4 magnetic nanoparticles (NPs) have been reported in the literatures [11–14], e.g. reduction of hematite by CO/CO_2 or H_2 [15], co-precipitation from the ferrous/ferric mixed solution in alkaline medium [16]. Recently, conventional hydrothermal method has been used to synthesize magnetite NPs by the reaction of ferric chloride and iron powder. In all these reported wet chemical methods, to get reproducible stoichiometric magnetite NPs, the critical control of various synthesis parameters [17,18], such as pH, temperature, Fe^{2+}/Fe^{3+} ratio, use of mild reducing agent, use of oxidant like KNO_3, etc., is necessary.

Soft ferrites such as Mn–Zn, Ni–Zn and Mg–Mn ferrites, are widely used in many fields [19,20]. Manganese zinc ferrites are technologically important materials because of their high magnetic permeability and low core losses. These ferrites have been widely used in electronic applications such as recording heads, choke coils, transformers, noise filters, etc. Ferrites are commonly produced by a ceramic process involving high temperature solid state reactions. The particles obtained by this process are rather large and non-uniform in size. These non-uniform particles result in the formation of voids or low density area in the green compacts. On sintering, non-reproducible products in terms of their magnetic property are obtained. In order to overcome the difficulties arising out of the ceramic route, wet chemical methods like air oxidation [21], co-precipitation [22,23], hydrothermal processing [24,25], etc., have been considered for the production of homogeneous, fine and reproducible ferrites. To synthesize pure, nanosized, relatively strain free Mn–Zn ferrites with narrow size distribution at a low reaction temperature, the hydrothermal processing attracts much attention in recent years [26–28]. However, the research about $Fe_3O_4/Mn_{0.8}Zn_{0.2}Fe_2O_4$ core/shell magnetic NPs has not been reported.

Various chemical methods have been applied for the production of NPs with narrow size distribution such as sol–gel processing, flame aerosol technique [29], solvothermal synthesis [30], micro-emulsion method, hot soap method and pulsed wire evaporation method [31]. The nanosized reactors, which were developed recently, have attracted much attention and can be used to produce NPs with narrow size distribution [32,33]. Besides, much attention

* Corresponding author at: College of Chemistry, Chemical Engineering and Materials Science, Soochow University, SIP, Suzhou 215123, China.
Tel.: +86 512 6588 0402; fax: +86 512 6588 0089.
E-mail address: rhong@suda.edu.cn (R.Y. Hong).

0925-8388/$ – see front matter © 2009 Elsevier B.V. All rights reserved.
doi:10.1016/j.jallcom.2009.02.098

has been paid to the simulation, kinetics and mechanism of the synthesis of NPs [34,35].

Co-precipitation is an easy and effective method to synthesize NPs. In the present investigation, Mn–Zn ferrite NPs were prepared by co-precipitation. Orthogonal tests ($L4^5$) were carried out to find the effects of OH^- and Fe^{3+} concentrations, and the temperature on the saturation magnetization of Mn–Zn ferrite NPs. The best reaction condition was obtained. Then, $Fe_3O_4/Mn_{0.8}Zn_{0.2}Fe_2O_4$ core/shell magnetic NPs were synthesized by co-precipitation under the same condition. The $Fe_3O_4/Mn_{0.8}Zn_{0.2}Fe_2O_4$ core/shell magnetic NPs reveal the highest saturation magnetization of 68 emu/g at the ratio of 2:1.

2. Experimental

2.1. Materials

Ferric chloride ($FeCl_3·6H_2O$), ferrous sulfate ($FeSO_4·7H_2O$), $MnCl_2·4H_2O$, zinc sulfate heptahydrate ($ZnSO_4·7H_2O$), sodium hydroxide (NaOH), hydrazine hydrate ($N_2H_4·H_2O$), and aqueous ammonia ($NH_3·H_2O$) used in the experiments are all analytic grade. Hydrochloric acid and sodium citrate are chemical grade. Ar is industrial grade. Deionized water was used throughout the experiments.

2.2. Synthesis of Fe_3O_4 magnetic NPs

The synthesis of Fe_3O_4 magnetic NPs was based on our previous studies [36], in which a mixed solution of $FeCl_3$ (0.5 M) and $FeSO_4$ (0.5 M) with a molar ratio of 1.75:1 was prepared under Ar protection. Then, 10 ml of ammonia aqueous solution was quickly dropped into the solution with vigorous stirring, followed by more ammonia aqueous solution and some hydrazine hydrate until the pH of the solution reached 9. Then, the solution was stirred for additional 30 min under Ar protection. Finally, the precipitates were collected by a magnet and washed several times with deionized water until the pH decreased to 7.0.

2.3. Sodium citrate modification of Fe_3O_4 NPs

The surface modification of Fe_3O_4 magnetic NPs was carried out, and the typical procedure was as follows: 1 g of Fe_3O_4 and 200 ml of sodium citrate (0.5 M) were mixed together in a flask. To reduce the aggregation of NPs, the mixture was kept in ultrasonic irradiation for 30 min. After that, the reaction mixture was stirred for 12 h at 60 °C under Ar protection. Then, the precipitates were collected by a magnet and washed with acetone to remove remnant sodium citrate.

2.4. Synthesis of $Mn_{1-x}Zn_xFe_2O_4$ NPs

2.4.1. Preparation procedure

The synthesis of $Mn_{1-x}Zn_xFe_2O_4$ NPs was carried out using OH^-, and the equation can be expressed as $(1-x)Mn^{2+} + xZn^{2+} + 2Fe^{3+} + 8OH^- \rightarrow Mn_{1-x}Zn_xFe_2O_4 + 4H_2O$, where x is the molar ratio of Zn^{2+}, and $0 < x < 1$.

The preparation process was as follows: the mixed solution of $MnCl_2$ (177 ml, 0.1 M), $ZnSO_4$ (10 ml, 0.5 M) and $FeCl_3$ (10 ml, see Table 1 for concentrations) was prepared. The solution was stirred at expectant temperature, and some dosage of NaOH solution was quickly added into the solution. Then, the solution was stirred for additional 1 h under Ar protection. Finally, the precipitate was collected by a magnet and washed several times with deionized water until the pH decreased to 7.0.

2.4.2. Orthogonal tests ($L4^5$)

A group of orthogonal tests ($L4^5$) was arranged to investigate the effects of reaction temperature, and OH^- and Fe^{3+} concentrations on the magnetic property of Mn–Zn ferrite, and the reaction time and aging time were set as constant, which is shown in Table 1. A series of experiments were carried out in sequence, as shown in Table 2. The saturation magnetizations of *Samples 1* to *16* were obtained.

Table 1
Factors of orthogonal tests ($L4^5$).

No.	Temperature (°C)	OH^- (mol L^{-1})	Fe^{3+} (mol L^{-1})	Reaction time (h)	Aging time (d)
1	55	1.0	0.5	1	3
2	75	2.0	1.0	1	3
3	95	4.0	1.2	1	3
4	115	5.0	1.5	1	3

Table 2
Results of orthogonal tests ($L4^5$).

No.	Temperature (°C)	OH^- (mol L^{-1})	Fe^{3+} (mol L^{-1})	Ms (emu g^{-1})
1	55	1.0	0.5	20
2	55	2.0	1.0	32
3	55	4.0	1.2	35
4	55	5.0	1.5	40
5	75	1.0	1.0	42
6	75	2.0	0.5	20
7	75	4.0	1.5	40
8	75	5.0	1.2	37
9	95	1.0	1.2	36
10	95	2.0	1.5	48
11	95	4.0	0.5	50
12	95	5.0	1.0	44
13	115	1.0	1.5	46
14	115	2.0	1.2	51
15	115	4.0	1.0	40
16	115	5.0	0.5	53

2.5. Preparation of $Fe_3O_4/Mn_{1-x}Zn_xFe_2O_4$ NPs

The sodium citrate modified magnetic NPs were re-dispersed in the mixed solution of $MnCl_2$, $ZnSO_4$ and $FeCl_3$, and the same process described in Section 2.4 was performed to synthesize Mn–Zn ferrite shell. The optimal preparation condition for Mn–Zn ferrite was obtained from a series of experiments according to the orthogonal tests ($L4^5$) in Section 2.4.2. Finally, five kinds of $Fe_3O_4/Mn_{0.8}Zn_{0.2}Fe_2O_4$ core/shell NPs were obtained with molar ratio of 3:1, 2:1, 1:1, 1:2 and 1:3, and are named as *Samples 1*, *2*, *3*, *4* and *5*, respectively. In the following analyses, *Sample 2* was characterized by a series of measurements.

2.6. Characterization

Fourier transform infrared (FT-IR) spectra were obtained using Nicolet FT-IR Avatar 360 (Nicolet, USA) with the KBr method. XPS analysis was conducted in PHI-5300 ESCA system (PerkinElmer, USA) at a power of 250 W, with Mg-Kα radiation. X-ray diffraction (XRD) measurements were carried out with D/Max-IIIC (Rigaku, Japan), using Cu-Kα radiation. The sizes of NPs were determined by a transmission electron microscope (TEM, Hitachi H-600-II, Japan). The size distribution of magnetic particles in water was obtained using a Malvern HPPS5001 laser particle-size analyzer. The magnetic property of NPs was measured by a vibrating sample magnetometer (VSM, EV7, ADE Co. of USA, with a precision of 0. 1) under room temperature.

3. Results and discussion

3.1. IR analysis

Fig. 1 shows the FT-IR spectra of sodium citrate coated-Fe_3O_4 (Fig. 1a) and $Fe_3O_4/Mn_{0.8}Zn_{0.2}Fe_2O_4$ core/shell NPs (Fig. 1b). The absorptions at 1589.9 and 1396.9 cm^{-1} in Fig. 1a can be assigned to the COO–Fe bond, and the peak at 578.8 cm^{-1} is the characteristic absorption of Fe–O bond. It reveals that sodium citrate has been grafted onto the surface of Fe_3O_4 NPs through the reaction of hydroxide radical groups (–OH) on the surface of Fe_3O_4 NPs and carboxylate anion (R–COO^-) of sodium citrate [37]. In Fig. 1b, the characteristic absorptions of COO–Fe bond and Fe–O bond still appear at 1620.3 and 1385.0 cm^{-1} and 460.0 cm^{-1}, respectively. Moreover, the characteristic absorption peaks of $Mn_{0.8}Zn_{0.2}Fe_2O_4$ NPs appear at 455.2 and 598.0 cm^{-1}, demonstrating that $Fe_3O_4/Mn_{0.8}Zn_{0.2}Fe_2O_4$ core/shell NPs are successfully synthesized.

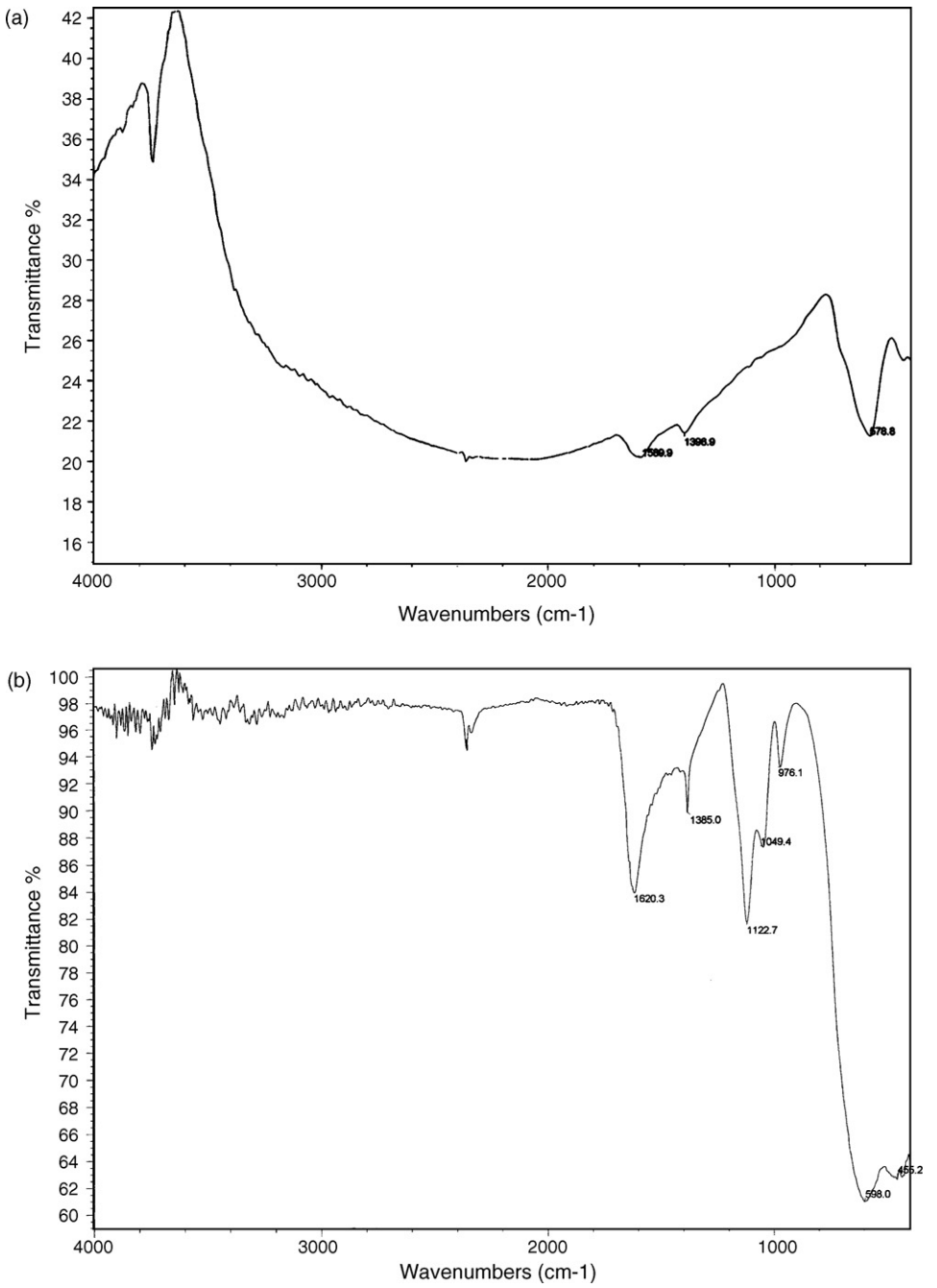

Fig. 1. FT-IR spectra of sodium citrate treated Fe_3O_4 NPs (a) and $Fe_3O_4/Mn_{0.8}Zn_{0.2}Fe_2O_4$ NPs (b).

3.2. Element analysis

According to the element analysis (not shown) using an accessory (EDS) of the HRTEM (JEM-2010, Jeol, Japan), the contents of different elements in *Sample 16* are determined as follows: Mn^{2+}: 8.68 at%, Zn^{2+}: 3.34 at%, Fe^{3+}: 30.81 at% and O^{2-}: 47.48 at%, which are shown in Table 3. It can be calculated that the obtained molecular formula is in accordance with $Mn_{0.8}Zn_{0.2}Fe_2O_4$.

The XPS spectra of $Mn_{0.8}Zn_{0.2}Fe_2O_4$ NPs and $Fe_3O_4/Mn_{0.8}Zn_{0.2}Fe_2O_4$ core/shell NPs (*Sample 2*) are shown in Fig. 2. The peaks of Mn from the two XPS spectra overlap, so do the peaks of Zn, Fe and O. The same intensity could be found when comparing the XPS spectrum of $Mn_{0.8}Zn_{0.2}Fe_2O_4$ with that of $Fe_3O_4/Mn_{0.8}Zn_{0.2}Fe_2O_4$. The result indicates that $Mn_{0.8}Zn_{0.2}Fe_2O_4$ NPs are completely coated onto the Fe_3O_4 NPs surfaces. XPS test also shows the atomic content of the nanocomposite surfaces: Mn 9.61%, Zn 2.4%, Fe 24.92% and O 46.61%. This indicates that the components of the nanocomposite surfaces are $Mn_{0.8}Zn_{0.2}Fe_2O_4$. The result agrees with the FT-IR analysis.

Table 3
Element contents in *Sample 16*.

Element	wt%	at%	at% (theoretically)
C	3.54	9.69	9.69
O	23.07	47.48	51.61
Mn	14.49	8.68	10.06
Fe	52.26	30.81	25.8
Zn	6.64	3.34	2.84

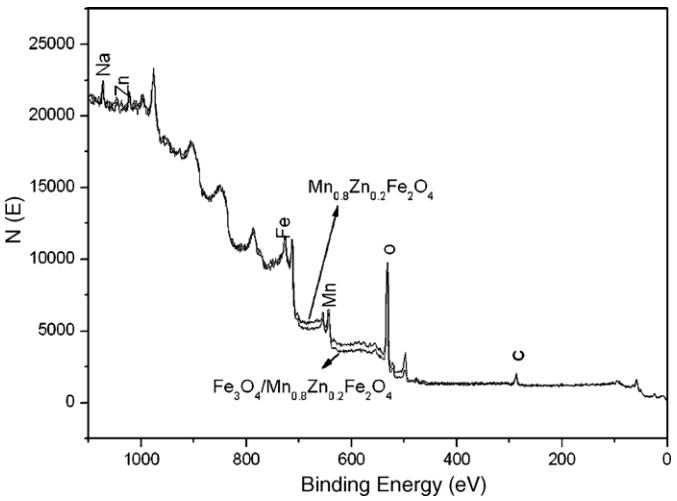

Fig. 2. XPS patterns of $Mn_{0.8}Zn_{0.2}Fe_2O_4$ and $Fe_3O_4/Mn_{0.8}Zn_{0.2}Fe_2O_4$ NPs.

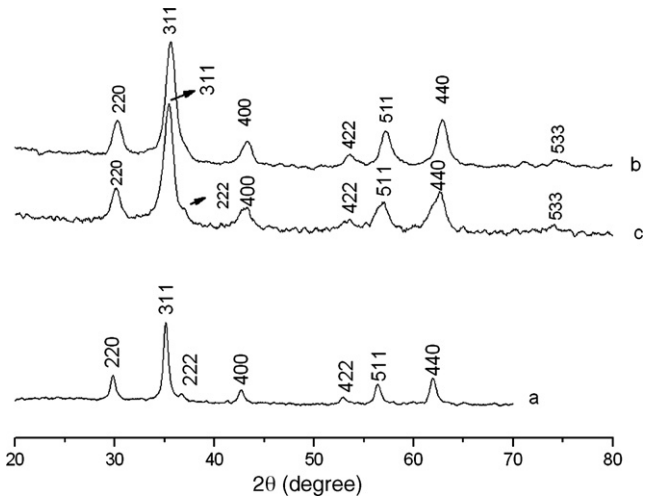

Fig. 3. XRD patterns of Fe_3O_4 NPs (a), $Mn_{0.8}Zn_{0.2}Fe_2O_4$ NPs (b) and $Fe_3O_4/Mn_{0.8}Zn_{0.2}Fe_2O_4$ core/shell NPs (c).

3.3. XRD analysis

Fig. 3 shows the X-ray powder diffraction patterns of Fe_3O_4 magnetic NPs (Fig. 3a), $Mn_{0.8}Zn_{0.2}Fe_2O_4$ NPs (Fig. 3b) and $Fe_3O_4/Mn_{0.8}Zn_{0.2}Fe_2O_4$ (Fig. 3c). A series of characteristic peaks in Fig. 3a at 2.968(2 2 0), 2.535(3 1 1), 2.103(4 0 0), 1.719(4 2 2), 1.614(5 1 1), 1.478(4 4 0) and 1.271(5 3 3) agree with the inverse cubic spinel phase of Fe_3O_4. The peaks are broadened because of tiny particle size. The average crystallite size D of the NPs

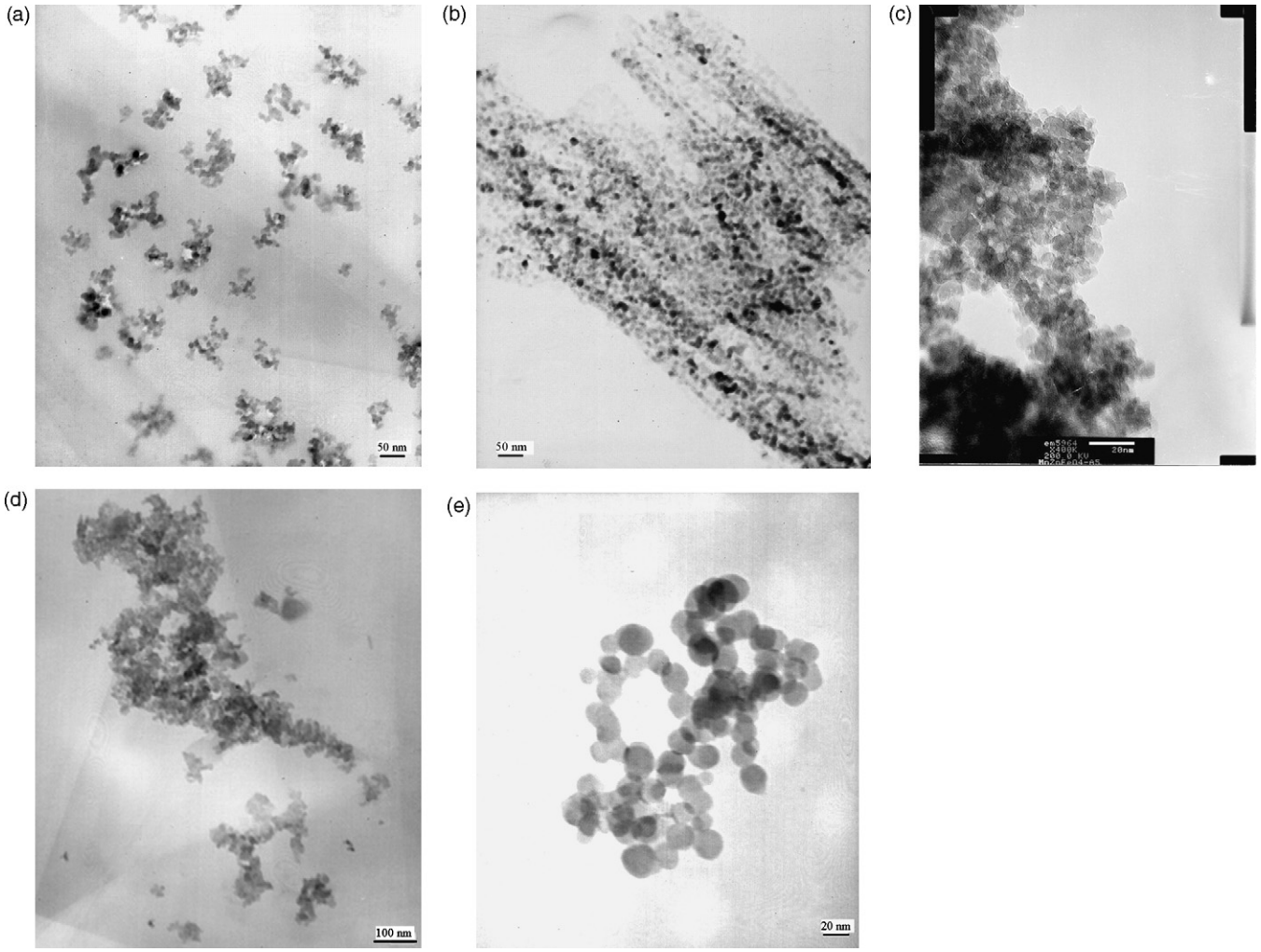

Fig. 4. TEM images of Fe_3O_4 magnetic NPs (a), sodium citrate coated-Fe_3O_4 magnetic NPs (b), $Mn_{0.8}Zn_{0.2}Fe_2O_4$ NPs (c), $Fe_3O_4/Mn_{0.8}Zn_{0.2}Fe_2O_4$ NPs (d) and sodium citrate coated-$Fe_3O_4/Mn_{0.8}Zn_{0.2}Fe_2O_4$ NPs (e).

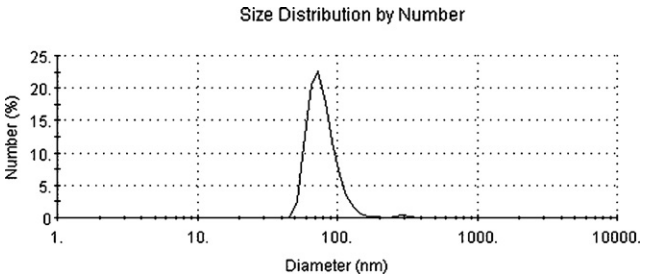

Fig. 5. Particle size distribution of *Sample 2*.

is about 10 nm, which was obtained from the Sherrer equation: $D = K\lambda/(\beta\cos\theta)$, where K is the Sherrer constant ($K = 0.89$), λ the X-ray wavelength (λ=1.5406 Å), β the peak width of half-maximum, and θ is the Bragg diffraction angle.

Fig. 3b shows the XRD pattern of Mn–Zn ferrite NPs. All peaks can be well indexed to $Mn_{0.8}Zn_{0.2}Fe_2O_4$. No other peaks of impurities are observed, suggesting that high-purity $Mn_{0.8}Zn_{0.2}Fe_2O_4$ NPs are obtained. The diameter D of $Mn_{0.8}Zn_{0.2}Fe_2O_4$ particles calculated using Sherrer equation is about 10 nm.

The XRD characteristic peaks of both Fe_3O_4 and $Mn_{0.8}Zn_{0.2}Fe_2O_4$ NPs can be found in Fig. 3c, which suggests that the crystalline structure of Fe_3O_4 NPs does not change after the modification with sodium citrate and coating with $Mn_{0.8}Zn_{0.2}Fe_2O_4$, and $Fe_3O_4/Mn_{0.8}Zn_{0.2}Fe_2O_4$ nanocomposites with core/shell structure are synthesized.

3.4. TEM analysis

The TEM photographs of Fe_3O_4 magnetic NPs before and after treatment with sodium citrate are shown in Fig. 4a and b, respectively. It is found that the dispersion of sodium citrate-modified Fe_3O_4 NPs is apparently better than that of untreated ones. This can be explained that after the treatment the surfaces of Fe_3O_4 NPs are negatively charged, and the aggregation is reduced due to the repulsion of electrostatic force. Besides, one can find that the normal size of Fe_3O_4 NPs is 10 nm, which is in accordance with the XRD analysis.

Fig. 4c shows the TEM micrograph of Mn–Zn ferrite NPs. Because of the large specific surface area, high surface energy, and dipolar attractive interactions of the magnetic NPs, some of the magnetic NPs congregated, such as the darker area in the micrograph. The NPs are rather polydispersed in size. Fig. 4c also illustrates that the

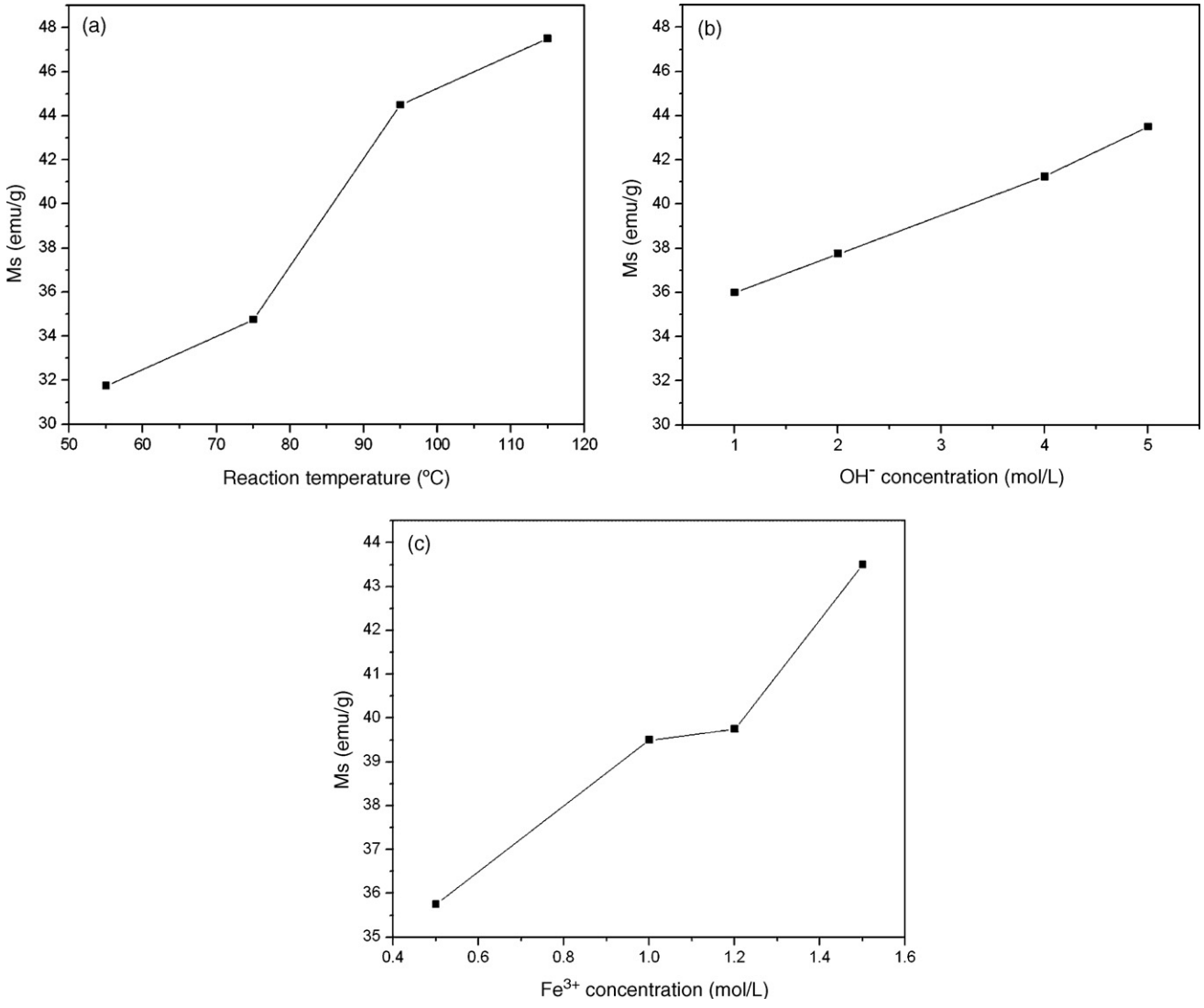

Fig. 6. Effects of reaction temperature (a), OH^- concentration (b) and Fe^{3+} concentration (c) on the saturation magnetization of Mn–Zn ferrite NPs.

Table 4
Analysis of orthogonal tests ($L4^5$) results.

	I	II	III	IV	Variability
Reaction temperature (°C)	31.75	34.75	44.50	47.50	15.75
OH^- concentration (mol/L)	36.0.	37.75	41.25	43.50	7.50
Fe^{3+} concentration (mol/L)	35.75	39.50	39.75	43.50	7.75

Note: The variability is the value of Ms (IV) minus Ms (I).

normal size of Mn–Zn ferrite NPs is about 10 nm, which matches the result obtained from XRD analysis very well.

Fig. 4d and e show the TEM photographs of unmodified Fe_3O_4 NPs coated with $Mn_{0.8}Zn_{0.2}Fe_2O_4$ and sodium citrate-treated Fe_3O_4 NPs coated with $Mn_{0.8}Zn_{0.2}Fe_2O_4$. The TEM photographs illustrate that the normal size of $Fe_3O_4/Mn_{0.8}Zn_{0.2}Fe_2O_4$ NPs is 30 nm, larger than that of Fe_3O_4 NPs (which is found to be about 10 nm). We can find in Fig. 4e that the dispersibility of NPs is much better than that in Fig. 4d. This indicates that the surface modification of Fe_3O_4 NPs has a great influence on the dispersibility of the nanoparticles. This is due to the remarkable increase in particle size from 10 nm (Fe_3O_4 NPs) to 30 nm ($Fe_3O_4/Mn_{0.8}Zn_{0.2}Fe_2O_4$ NPs), the specific surface area, surface energy, and dipolar attractive interactions of the NPs are reduced greatly.

3.5. Particle size distribution

The size distribution of *Sample 2* dispersed in water is shown in Fig. 5. The value of $d\ (0.98)_{num}$ of *Sample 2* indicates that the mean size of $Fe_3O_4/Mn_{0.8}Zn_{0.2}Fe_2O_4$ core/shell NPs in volume is 78.47 nm. The mean size determined by the laser particle-size analyzer is larger than that by the TEM and XRD analysis. That is because the size distribution measurement reveals the sizes of both particles and aggregates if existed, while the TEM and XRD analysis only show the sizes of particles. Generally, it is inevitable for aggregations existed in the NPs powders, leading to the larger mean size shown by the laser particle-size analyzer.

3.6. Optimal conditions for synthesis of $Mn_{0.8}Zn_{0.2}Fe_2O_4$

Table 4 is obtained by analyzing the data in Table 2 according to the orthogonal tests. Among the three factors in Table 4, the reaction temperature has the maximal variability indicating it has the greatest effect on the saturation magnetization of Mn–Zn ferrite. The variability of OH^- and Fe^{3+} concentration are the same, implying that the two factors have little effect on the saturation magnetization of Mn–Zn ferrite. According to the orthogonal tests, when only one factor is considered, the change of saturation magnetization can be obtained, as shown in Fig. 6. The slope of Fig. 6a is larger than that of Fig. 6b and c, suggesting that the reaction temperature has the greatest effect on the saturation magnetization of Mn–Zn ferrite. This can be explained by the fact that higher reaction temperature is propitious to better crystalline structure. Our previous investigations have proved that different synthesis conditions, such as reaction temperature, OH^- concentration, etc., directly affected the crystalline and particle size, and that better crystal is related to higher magnetization [38]. Therefore, the best reaction condition obtained here is the OH^- concentration of 5 mol/L, the Fe^{3+} concentration of 0.5 mol/L and the temperature at 115 °C.

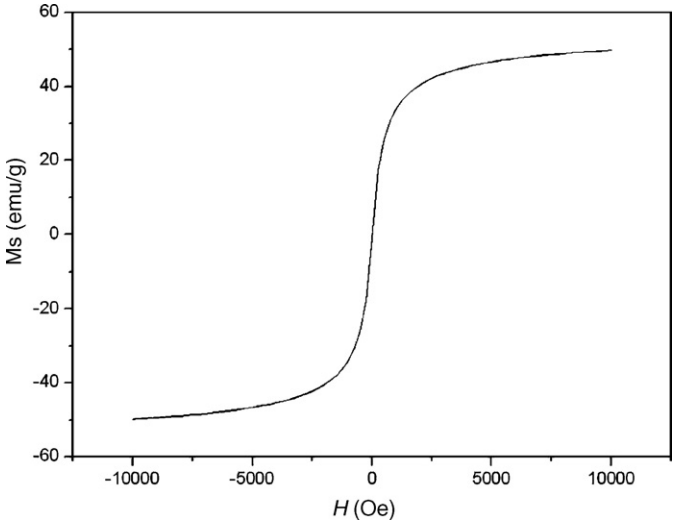

Fig. 8. Magnetic hysteresis curve of $Mn_{0.8}Zn_{0.2}Fe_2O_4$ NPs.

3.7. Magnetic property

The magnetic property of Fe_3O_4 NPs is shown in Fig. 7. It demonstrates that the coercivity of the NPs is 40.25 Oe, and the saturation magnetization (Ms) is 60 emu/g. The saturation magnetization (Ms) of *Sample 1* to *16* is listed in Table 2, and *Sample 16* has the highest saturation magnetization of 53 emu/g. The magnetic hysteresis curve of *Sample 16* is shown in Fig. 8, and one can find that the

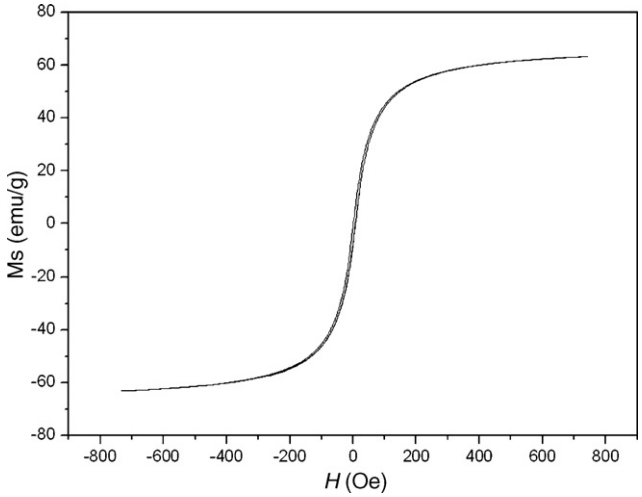

Fig. 7. Magnetic hysteresis curve of Fe_3O_4 magnetic NPs.

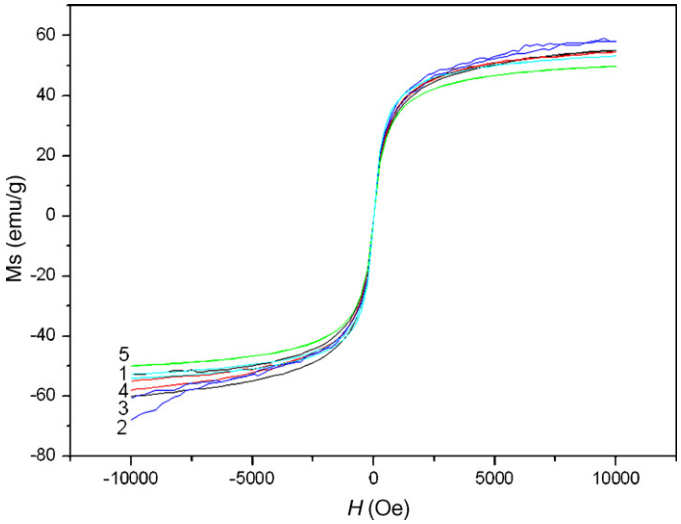

Fig. 9. Magnetic hysteresis curves of $Fe_3O_4/Mn_{0.8}Zn_{0.2}Fe_2O_4$ NPs.

synthesized $Mn_{0.8}Zn_{0.2}Fe_2O_4$ NPs (*Sample 16*) demonstrate superparamagnetism. The decrease of saturation magnetization can be attributed to the substitution of Fe^{3+} by Mn^{2+} and Zn^{2+}.

The magnetic hysteresis curves of $Fe_3O_4/Mn_{0.8}Zn_{0.2}Fe_2O_4$ NPs are shown in Fig. 9. It could be seen from the five loops that all the $Fe_3O_4/Mn_{0.8}Zn_{0.2}Fe_2O_4$ NPs are superparamagnetic and the saturation magnetization (Ms) of *Sample 1* to *5* is 55, 68, 61, 59 and 51 emu/g, respectively. The saturation magnetization of *Sample 2* is 68 emu/g, which is higher than other core/shell NPs. This could be ascribed to the strong interaction between magnetic hard phase (Fe_3O_4) and soft phase ($Mn_{0.8}Zn_{0.2}Fe_2O_4$) when at the molar ratio of 2:1.

4. Conclusions

After the chemical synthesis and physical characterization, the following conclusions can be drawn:

(1) The inverse cubic spinel phase of Fe_3O_4 NPs with a diameter of about 10 nm and with saturation magnetization of 60 emu/g were synthesized by the co-precipitation of Fe^{3+} and Fe^{2+} with ammonium hydroxide under hydrazine hydrate.
(2) High purity $Mn_{0.8}Zn_{0.2}Fe_2O_4$ NPs with a diameter of 10 nm were obtained by co-precipitation of Mn^{2+}, Zn^{2+} and Fe^{3+}. The highest saturation magnetization is 53 emu/g. The reaction temperature was found to have important effect on the saturation magnetization of Mn–Zn ferrite. The best reaction conditions obtained by orthogonal experiments ($L4^5$) are: OH^- concentration of 5 mol/L, Fe^{3+} concentration of 0.5 mol/L and reaction temperature at 115 °C.
(3) $Mn_{0.8}Zn_{0.2}Fe_2O_4$ were successfully coated onto the Fe_3O_4 NPs. The diameter of the $Fe_3O_4/Mn_{0.8}Zn_{0.2}Fe_2O_4$ core/shell NPs is about 30 nm, and the $Fe_3O_4/Mn_{0.8}Zn_{0.2}Fe_2O_4$ core/shell NPs have the highest saturation magnetization of 68 emu/g when the molar ration of Fe_3O_4 to $Mn_{0.8}Zn_{0.2}Fe_2O_4$ is 2:1.
(4) The Fe_3O_4 magnetic NPs treated by sodium citrate show better dispersibility, and the treated Fe_3O_4 NPs can be coated by $Mn_{0.8}Zn_{0.2}Fe_2O_4$ uniformly. The surface modification of Fe_3O_4 NPs by sodium citrate can improve the surface coating effectively.

Acknowledgment

The project was supported by the National Natural Science Foundation of China (NNSFC, Nos. 20876100 and 20736004), National Program on Key Basic Research Project (973 Program 2009CB219904), the State Key Laboratory of Multi-phase Complex Systems, Institute of Process Engineering, Chinese Academy of Sciences (No. 2006-5), the Key Laboratory of Organic Synthesis of Jiangsu Province and R&D Foundation of Nanjing Medical University (NY0586).

References

[1] M. Fofana, M.S. Kuma, Miner. Met. Rev. 38 (4) (1997) 35–40.
[2] K. Nakatsuka, B. Jeyadevan, S. Neveu, J. Magn. Magn. Mater. 252 (2002) 360–362.
[3] Y.B. Khollam, S.R. Dhage, H.S. Potdar, J. Magn. Magn. Mater. 56 (2002) 571–577.
[4] D.L. Zhao, X.W. Zeng, Q.S. Xia, J.T. Tang, J. Alloys Compd. 469 (1–2) (2009) 215–218.
[5] A. Jordan, R. Scholz, P. Wust, H. Fähling, R. Felix, J. Magn. Magn. Mater. 201 (1999) 413–419.
[6] Y. Zhang, N. Kohler, M.Q. Zhang, Biomaterials 23 (2002) 1553–1561.
[7] E.H. Kim, Y. Ahn, H.S. Lee, J. Alloys Compd. 434–435 (2007) 633–636.
[8] B. Feng, R.Y. Hong, Y.J. Wu, G.H. Liu, L.H. Zhong, Y. Zheng, J.M. Ding, D.G. Wei, J. Alloys Compd. 473 (1–2) (2009) 356–362.
[9] L. Shen, P.E. Laibinis, T.A. Hatton, Langmuir 15 (1999) 447–453.
[10] Q. Li, Y.M. Xuan, J. Wang, Exp. Therm. Fluid Sci. 30 (2005) 109–116.
[11] L.S. Darken, R.W. Gurry, J. Am. Chem. Soc. 68 (1946) 798–816.
[12] M. Ma, Y. Zhang, W. Yu, Colloids Surf. A: Physicochem. Eng. Aspects 212 (2003) 219–226.
[13] F.Y. Cheng, C.H. Su, Y.S. Yang, Biomaterials 26 (2005) 729–738.
[14] Z.X. Yue, J. Zhou, H.G. Zhang, J. Chin. Ceramic Soc. 27 (4) (1999) 466–470.
[15] L.S. Darken, H.F. Meier, J. Am. Chem. Soc. 64 (1942) 621–623.
[16] G. Visalakshi, G. Venkateswaran, S.K. Kulshreshtha, P.N. Moorthy, Mater. Res. Bull. 28 (1993) 829–836.
[17] R. Arulmurugan, G. Vaidyanathan, Physica B 368 (2005) 223–230.
[18] M. Kiyama, Bull. Chem. Soc. Jpn. 47 (1974) 1646–1651.
[19] L.Q. Yu, L.J. Zheng, J.X. Yang, Mater. Chem. Phys. 66 (1) (2000) 6–9.
[20] P. Wang, C.F. Lee, T. Young, J. Polym. Sci. Part A: Polym. Chem. 43 (2005) 1342–1356.
[21] M. Sisk, I. Kilbride, A.J. Barker, J. Mater. Sci. Lett. 14 (1995) 153–158.
[22] A. Ataie, M.R. Piramoon, I.R. Harris, C.B. Ponton, J. Mater. Sci. 30 (1995) 5600–5606.
[23] V.V. Pankov, M. Pernet, P. Germi, P. Molard, J. Magn. Magn. Mater. 120 (1993) 69–72.
[24] H. Kumazawa, Y. Maeda, E. Sada, J. Mater. Sci. Lett. 14 (1995) 68–73.
[25] Y. Yamamoto, A. Makino, J. Magn. Magn. Mater. 133 (1994) 500–508.
[26] D. Barb, L. Diamandescu, J. Mater. Sci. 21 (1986) 1118–1126.
[27] B. Skołyszewska, W. Tokarz, K. Przybylski, Z. Kakol, Physica C 387 (2003) 290–294.
[28] M. Maiorov, E. Blums, M. Hanson, C. Johanson, J. Magn. Magn. Mater. 201 (1999) 95–97.
[29] G.D. Ulrich, Chem. Eng. News 62 (1984) 22–27.
[30] A.G. Yan, X.H. Liu, G.Z. Qiu, H.Y. Wu, R. Yi, N. Zhang, J. Xu, J. Alloys Compd. 458 (2008) 487–491.
[31] H.M. Lee, Y.R. Uhm, C.K. Rhee, J. Alloys Compd. 461 (2008) 604–607.
[32] M. Takagi, T. Maki, M. Miyahara, K. Mae, Chem. Eng. J. 101 (2004) 269–276.
[33] J. Wagner, T. Kirner, G. Mayer, J. Albert, J.M. Köhler, Chem. Eng. J. 101 (2004) 251–260.
[34] L.G. Wang, R.O. Fox, Chem. Eng. Sci. 58 (2003) 4387–4401.
[35] E. Bilgili, R. Hamey, B. Scarlett, Chem. Eng. Sci. 61 (2006) 149–157.
[36] R.Y. Hong, J.H. Li, H.Z. Li, J. Ding, Y. Zheng, D.G. Wei, J. Magn. Magn. Mater. 320 (2008) 1605–1614.
[37] R.Y. Hong, S.Z. Zhang, Y.P. Han, H.Z. Li, J. Ding, Y. Zheng, Powder Technol. 170 (2006) 1–11.
[38] R.Y. Hong, T.T. Pan, H.Z. Li, J. Magn. Magn. Mater. 303 (2006) 60–68.